Limitations of Data-Driven Spectral Reconstruction: An Optics-Aware Analysis – Supplementary Material

Qiang Fu*, Matheus Souza*, Eunsue Choi, Suhyun Shin, Seung-Hwan Baek, Wolfgang Heidrich *Fellow, IEEE*

I. Aberrated Spectral PSFs

In Supplemental Fig. S1, we show the schematic optical layout of the double Gauss lens [8] we use throughout the experiments. It consists of 6 lens elements with an aperture stop in the middle. The effective focal length is 50 mm, and the F-number is F/1.8. We model the spectral PSFs at each wavelength in the spectral range [400 nm, 700 nm] with a step size of 10 nm in the optical design software ZEMAX (v14.2) by spectral ray tracing. The sensor parameters are set according to the specifications of Basler ace 2 camera (model A2a5320-23ucBAS), as used in the NTIRE 2022 spectral recovery challenge [2]. In Supplemental Fig. S1, we render the corresponding spectral PSFs in color with the SRF of that sensor. Although the lens is well designed to minimize all kinds of aberrations, clear chromatic aberrations can still be observed, in particular in the short (blue) and long (red) ends of the spectral bands. It is impossible to completely *eliminate* aberrations in photographic lenses [6], [13]. Note that all the spectral PSFs are normalized by their own maximum values for visualization purpose only.

II. Results of Training with Less Data for Other Networks

In Table 2 of the main paper, we summarize that the performance of all the candidate networks on the ARAD1K dataset is mildly affected by using only half of the training data. The detailed validation results over the course of training are shown in Supplemental Fig. S2 and Fig. S3. Here we show extended experimental results for the effects of training with 100%, 50%, and 20% of the full training data. All the results consistently support our indication of lack of diversity in the dataset.

III. Results of Validation with Unseen Data for Other Networks

In Table 3 of the main paper, we demonstrate the performance drop behaviour of the MST++ network on the ARAD1K dataset. To prove that this is true to other networks as well, we carry out the same experiments for all the other candidate networks. The results are summarized in Supplemental Table S.I and Supplemental Table S.II. As the noise levels, RGB formats, and aberration conditions asymptotically approach realistic imaging scenarios in the real world, the pre-trained models [4] for other networks gradually degrade, similar as the MST++. All the results consistently support our conclusion about the generalization difficulties of these methods in realistic imaging conditions.

IV. Results of Cross-Dataset Validation for Other Networks

As shown in Table 4 in the main paper, we demonstrate that the MST++ network has difficulties in keeping high performance when it is trained on one dataset and validated on another dataset. In Supplemental Table S.III and Supplemental Table S.IV, we show with extended experimental results that the effects of cross-dataset validation are true for all other networks as well. Similar cross-dataset failure can be observed for all the candidate networks. These results consistently support our conclusion about the important roles of scene content and acquisition devices in different datasets.

V. Results of Metamer Failure for Other Datasets

In Table 6 of the main paper, we compare the performance of the candidate networks for the standard data (no metamers), fixed metamers ($\alpha = 0$), and on-the-fly metamers (α varies in the range of [-1, 2] during training) synthesized from the ARAD1K dataset. All the metrics degrade significantly in the presence of metamers. In Supplemental Table S.V, Table S.VI and Table S.VII, we further show that this is also true for all the networks on the CAVE [14], ICVL [1], and KAUST [10] datasets. All the results consistently support our conclusion that existing methods cannot distinguish metamers, regardless of the network architectures and datasets.

VI. Results of the Aberration Advantage for Other Networks and Other Datasets

In Fig. 4 of the main paper, we demonstrate that it is beneficial to incorporate the realistic chromatic aberrations of the optical system into the training pipeline, such that the spectral accuracy can be improved. To prove that this phenomenon is regardless of the network architectures, we perform the same experiment for the other candidate networks on the ARAD1K dataset. The results are shown in Supplemental Fig. S5, Fig. S6 and Fig. S7.

We also demonstrate that the aberration advantage applies to other datasets. Since the MST++ network performs consistently among the top-performing architectures, we conduct the same experiments with this network on the CAVE, ICVL, and KAUST datasets. The results are shown in Supplemental Fig. S8. All the results clearly support our conclusion that the chromatic aberrations encode spectral information into the RGB images for the networks to effectively learn the embedded spectra.

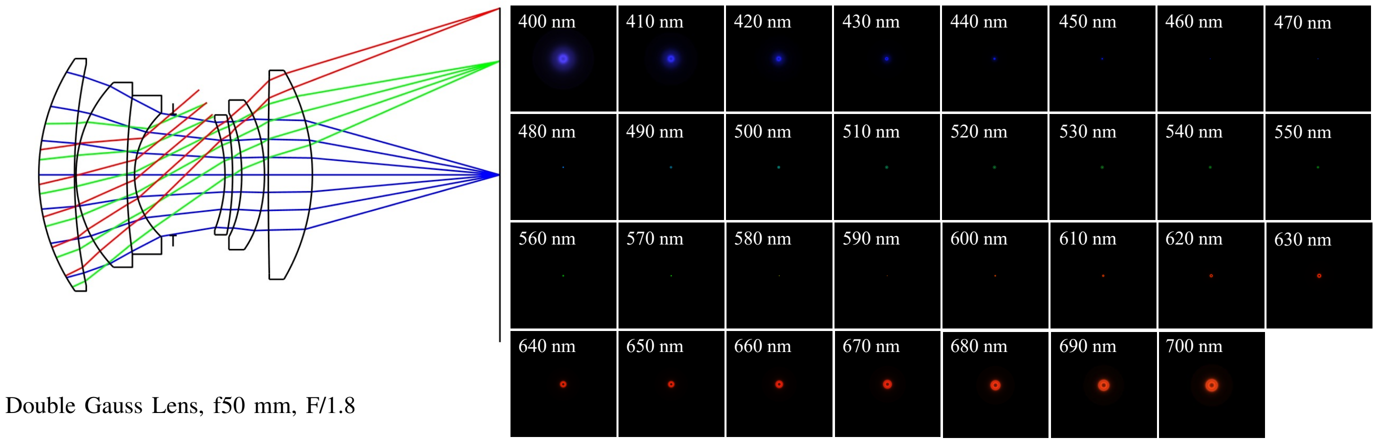

Fig. S1: Double Gauss lens layout (left) and its aberrated spectral PSFs (right). Lens data is obtained from [8] (Numerical Example 2). Spectral PSFs are modeled in optical design software ZEMAX and rendered in color for the Basler ace 2 camera (model A2a5320-23ucBAS) sensor. Clear chromatic aberrations can be observed throughout the spectral range.

References

[1] Boaz Arad and Ohad Ben-Shahar. Sparse recovery of hyperspectral signal from natural RGB images. In *Eur. Conf. Comput. Vis.*, pages 19–34. Springer, 2016.

[2] Boaz Arad, Radu Timofte, Rony Yahel, Nimrod Morag, Amir Bernat, Yuanhao Cai, Jing Lin, Zudi Lin, Haoqian Wang, Yulun Zhang, et al. NTIRE 2022 spectral recovery challenge and data set. In *IEEE Conf. Comput. Vis. Pattern Recog. Worksh.*, pages 863–881, 2022.

[3] Yuanhao Cai, Jing Lin, Xiaowan Hu, Haoqian Wang, Xin Yuan, Yulun Zhang, Radu Timofte, and Luc Van Gool. Mask-guided spectral-wise transformer for efficient hyperspectral image reconstruction. In *IEEE Conf. Comput. Vis. Pattern Recog.*, pages 17502–17511, 2022.

[4] Yuanhao Cai, Jing Lin, Zudi Lin, Haoqian Wang, Yulun Zhang, Hanspeter Pfister, Radu Timofte, and Luc Van Gool. MST++: Multi-stage spectral-wise transformer for efficient spectral reconstruction. In *IEEE Conf. Comput. Vis. Pattern Recog. Worksh.*, pages 745–755, 2022.

[5] Liangyu Chen, Xin Lu, Jie Zhang, Xiaojie Chu, and Chengpeng Chen. HINet: Half instance normalization network for image restoration. In *IEEE Conf. Comput. Vis. Pattern Recog.*, pages 182–192, 2021.

[6] Robert Edward Fischer, Biljana Tadic-Galeb, Paul R Yoder, Ranko Galeb, Bernard C Kress, Stephen C McClain, Tom Baur, Richard Plympton, Bob Wiederhold, and Bob Grant Alastair J. *Optical system design*, volume 599. Citeseer, 2000.

[7] Xiaowan Hu, Yuanhao Cai, Jing Lin, Haoqian Wang, Xin Yuan, Yulun Zhang, Radu Timofte, and Luc Van Gool. HDNet: High-resolution dual-domain learning for spectral compressive imaging. In *IEEE Conf. Comput. Vis. Pattern Recog.*, pages 17542–17551, 2022.

[8] Junya Ichimura. Optical system and image pickup apparatus having the same, August 2021. US Patent App. 17/174,832.

[9] Jiaojiao Li, Chaoxiong Wu, Rui Song, Yunsong Li, and Fei Liu. Adaptive weighted attention network with camera spectral sensitivity prior for spectral reconstruction from RGB images. In *IEEE Conf. Comput. Vis. Pattern Recog. Worksh.*, pages 462–463, 2020.

[10] Yuqi Li, Qiang Fu, and Wolfgang Heidrich. Multispectral illumination estimation using deep unrolling network. In *Int. Conf. Comput. Vis.*, pages 2672–2681, 2021.

[11] Bee Lim, Sanghyun Son, Heewon Kim, Seungjun Nah, and Kyoung Mu Lee. Enhanced deep residual networks for single image super-resolution. In *IEEE Conf. Comput. Vis. Pattern Recog. Worksh.*, pages 136–144, 2017.

[12] Zhan Shi, Chang Chen, Zhiwei Xiong, Dong Liu, and Feng Wu. HSCNN+: Advanced CNN-based hyperspectral recovery from RGB images. In *IEEE Conf. Comput. Vis. Pattern Recog. Worksh.*, pages 939–947, 2018.

[13] Warren J Smith. *Modern optical engineering: the design of optical systems*. McGraw-Hill Education, 2008.

[14] Fumihito Yasuma, Tomoo Mitsunaga, Daisuke Iso, and Shree K Nayar. Generalized assorted pixel camera: postcapture control of resolution, dynamic range, and spectrum. *IEEE Trans. Image Process.*, 19(9):2241–2253, 2010.

[15] Syed Waqas Zamir, Aditya Arora, Salman Khan, Munawar Hayat, Fahad Shahbaz Khan, and Ming-Hsuan Yang. Restormer: Efficient transformer for high-resolution image restoration. In *IEEE Conf. Comput. Vis. Pattern Recog.*, pages 5728–5739, 2022.

[16] Syed Waqas Zamir, Aditya Arora, Salman Khan, Munawar Hayat, Fahad Shahbaz Khan, Ming-Hsuan Yang, and Ling Shao. Learning enriched features for real image restoration and enhancement. In *Eur. Conf. Comput. Vis.*, pages 492–511. Springer, 2020.

[17] Syed Waqas Zamir, Aditya Arora, Salman Khan, Munawar Hayat, Fahad Shahbaz Khan, Ming-Hsuan Yang, and Ling Shao. Multi-stage progressive image restoration. In *IEEE Conf. Comput. Vis. Pattern Recog.*, pages 14821–14831, 2021.

[18] Yuzhi Zhao, Lai-Man Po, Qiong Yan, Wei Liu, and Tingyu Lin. Hierarchical regression network for spectral reconstruction from RGB images. In *IEEE Conf. Comput. Vis. Pattern Recog. Worksh.*, pages 422–423, 2020.

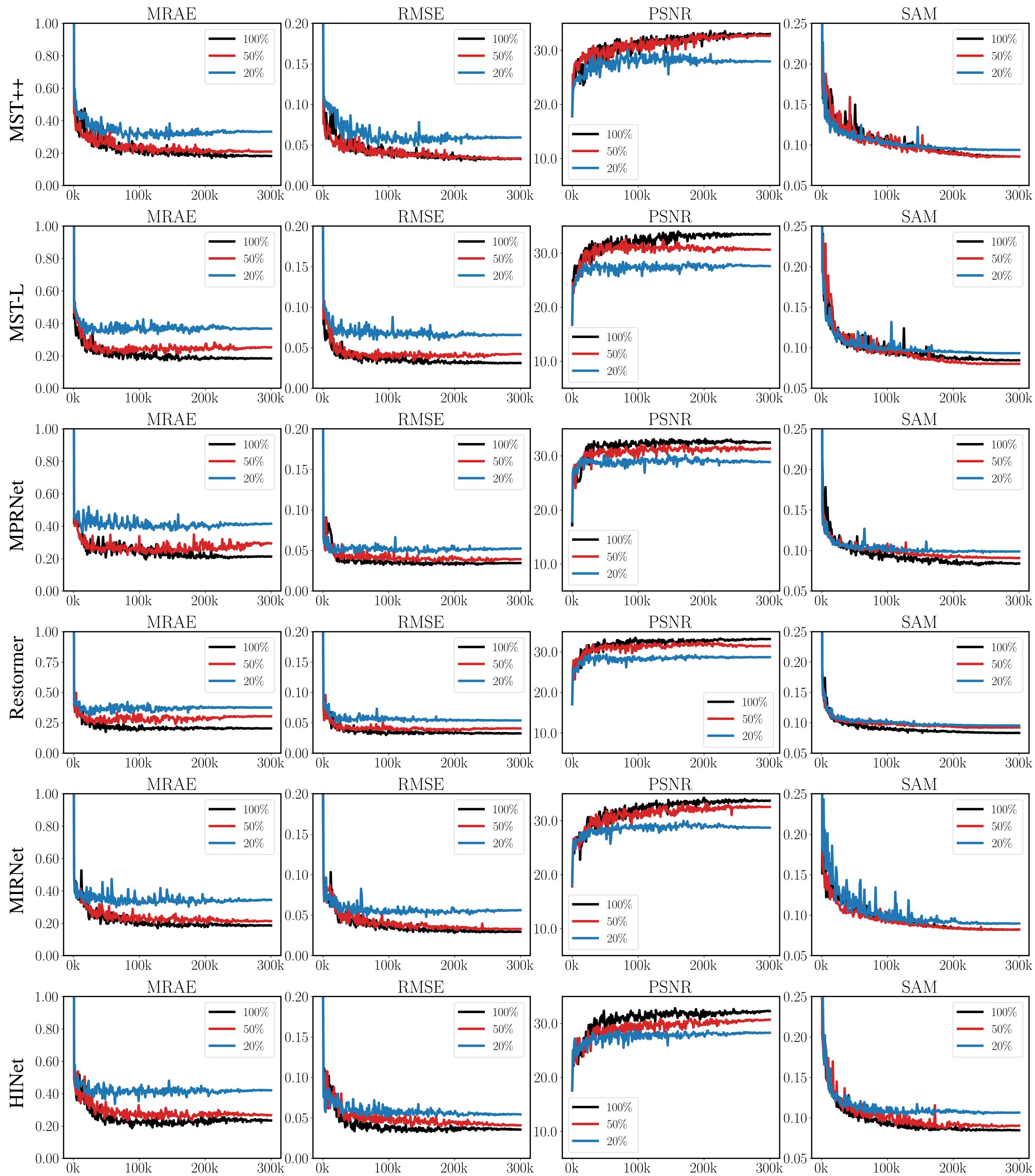

Fig. S2: Performance evaluation on MRAE, RMSE, PSNR, and SAM for MST++ [4], MST-L [3], MPRNet [17], Restormer [15], MIRNet [16], and HINet [5] with 100%, 50%, and 20% of the original training data on the ARAD1K dataset.

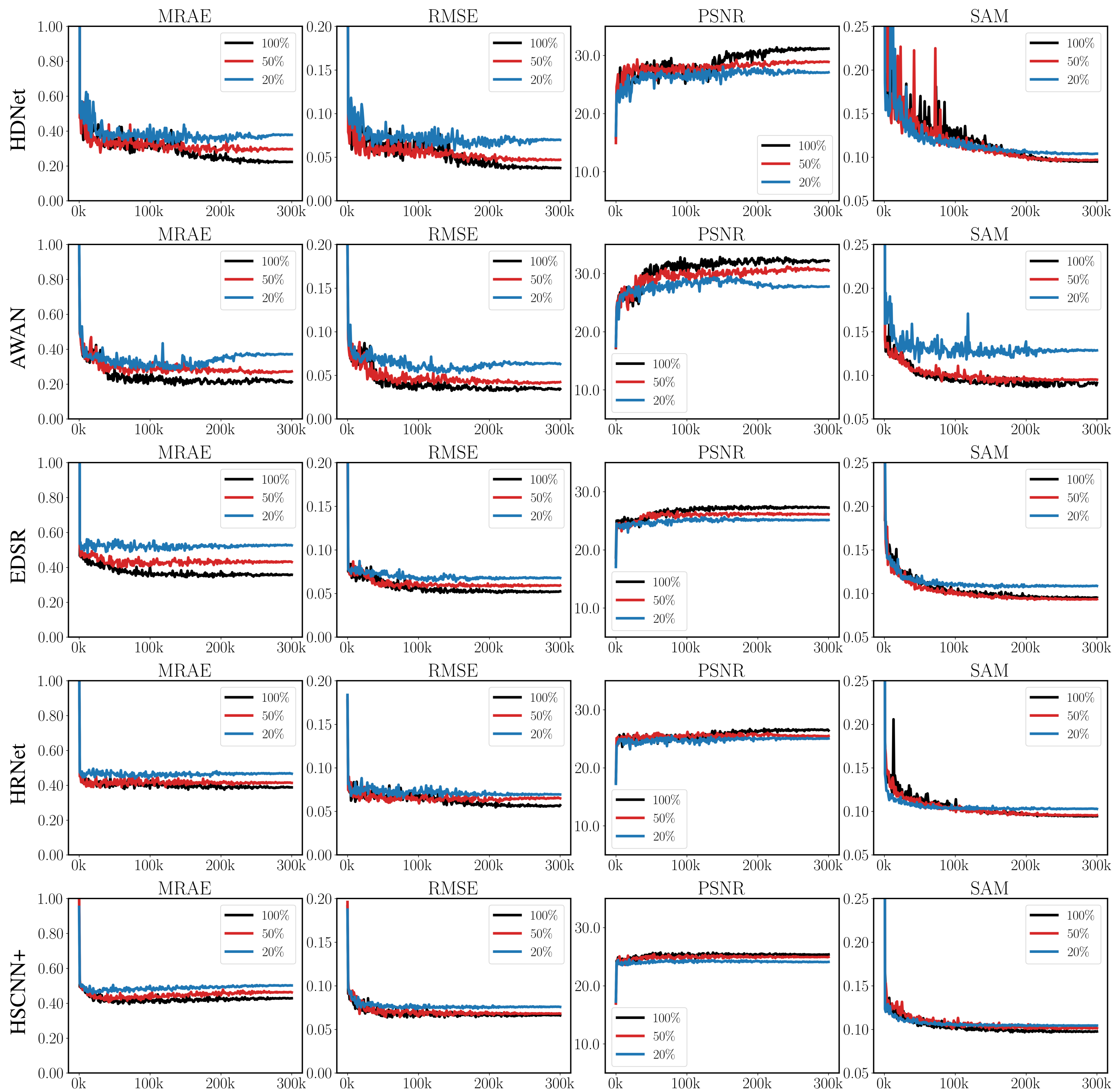

Fig. S3: Performance evaluation on MRAE, RMSE, PSNR, and SAM for HDNet [7], AWAN [9], EDSR [11], HRNet [18], and HSCNN+ [12] with 100%, 50%, and 20% of the original training data on the ARAD1K dataset.

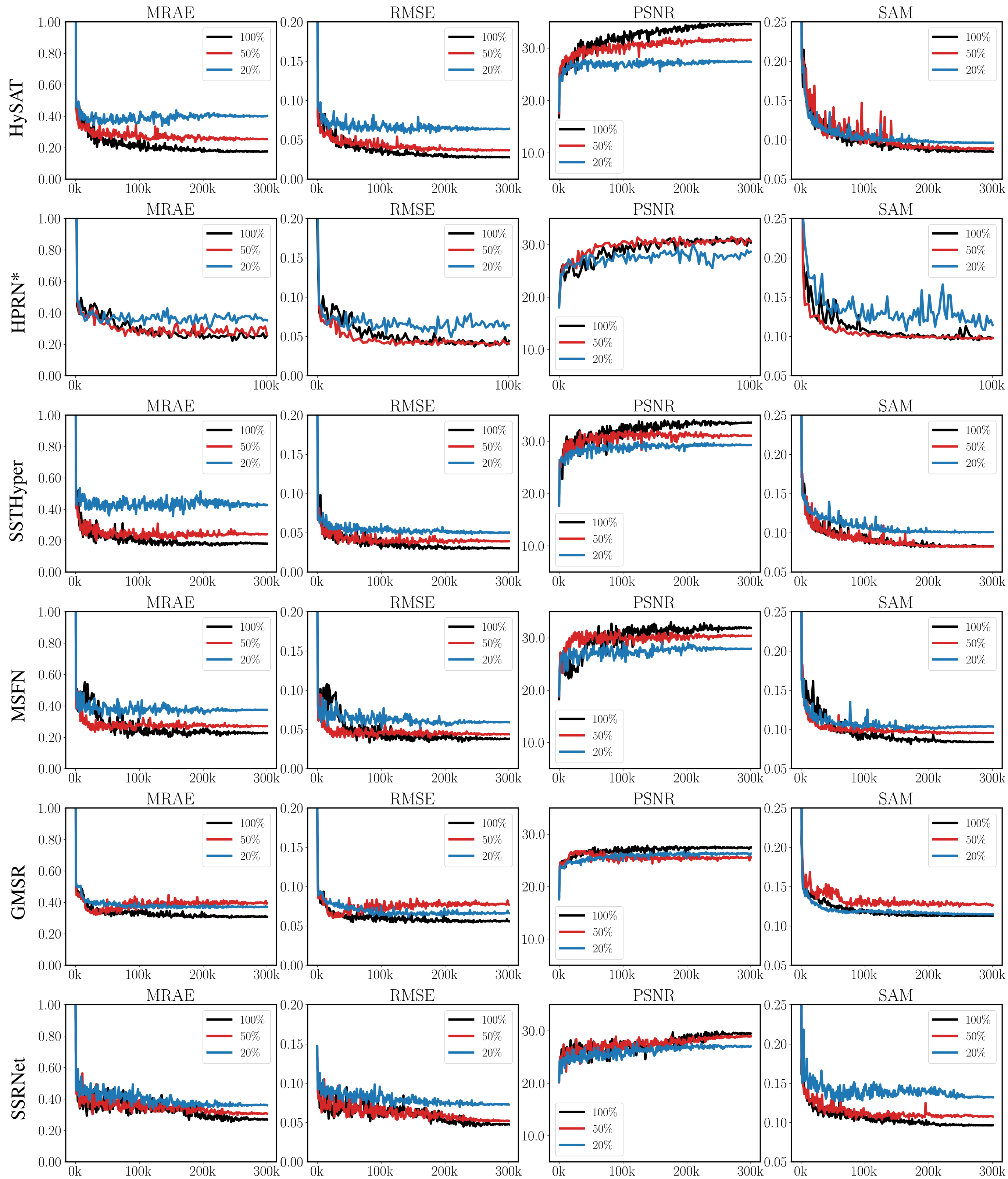

Fig. S4: Performance evaluation on MRAE, RMSE, PSNR, and SAM for HySAT, HPRN, SSTHyper, MSFN, GMSR, and SSRNet with 100%, 50%, and 20% of the original training data on the ARAD1K dataset. * Note: HPRN was originally not trained on ARAD1K. We followed the training strategy in the original paper, but the results diverged after around 100k iterations, so we reported the results only up to 100k iterations when the convergence was observed.

TABLE S.I: Evaluation of pre-trained models on synthesized validation data generated from the ARAD1K dataset (Part I).

Network	Data property				MRAE ↓	RMSE ↓	PSNR ↑	SAM ↓
	Data source	Noise (npe)	RGB format	Aberration				
MST++	NTIRE 2022	unknown	jpg (Q unknown)	None	0.170	0.029	33.8	0.084
	Synthesized	0	jpg (Q = 65)	None	0.460	0.049	29.2	0.094
		0	png (lossless)	None	0.362	0.057	28.7	0.087
		1000	png (lossless)	CA*	0.312	0.055	28.4	0.118
MST-L	NTIRE 2022	unknown	jpg (Q unknown)	None	0.181	0.031	33.0	0.091
	Synthesized	0	jpg (Q = 65)	None	0.417	0.047	29.7	0.099
		0	png (lossless)	None	0.384	0.058	28.4	0.096
		1000	png (lossless)	CA*	0.327	0.055	28.0	0.118
MPRNet	NTIRE 2022	unknown	jpg (Q unknown)	None	0.182	0.032	32.9	0.088
	Synthesized	0	jpg (Q = 65)	None	0.453	0.048	29.1	0.092
		0	png (lossless)	None	0.359	0.051	29.5	0.086
		1000	png (lossless)	CA*	0.661	0.066	26.1	0.125
Restormer	NTIRE 2022	unknown	jpg (Q unknown)	None	0.190	0.032	33.0	0.097
	Synthesized	0	jpg (Q = 65)	None	0.454	0.051	28.6	0.100
		0	png (lossless)	None	0.363	0.053	28.6	0.098
		1000	png (lossless)	CA*	0.510	0.066	25.5	0.126
MIRNet	NTIRE 2022	unknown	jpg (Q unknown)	None	0.189	0.032	33.3	0.091
	Synthesized	0	jpg (Q = 65)	None	0.467	0.051	28.7	0.096
		0	png (lossless)	None	0.366	0.055	28.8	0.091
		1000	png (lossless)	CA*	0.404	0.077	24.8	0.124
HINet	NTIRE 2022	unknown	jpg (Q unknown)	None	0.212	0.037	31.4	0.091
	Synthesized	0	jpg (Q = 65)	None	0.460	0.051	28.3	0.094
		0	png (lossless)	None	0.384	0.055	28.2	0.094
		1000	png (lossless)	CA*	0.450	0.063	26.5	0.120
HDNet	NTIRE 2022	unknown	jpg (Q unknown)	None	0.214	0.037	31.5	0.098
	Synthesized	0	jpg (Q = 65)	None	0.404	0.050	28.8	0.102
		0	png (lossless)	None	0.395	0.057	28.0	0.096
		1000	png (lossless)	CA*	0.450	0.082	23.9	0.126
AWAN	NTIRE 2022	unknown	jpg (Q unknown)	None	0.222	0.041	31.0	0.098
	Synthesized	0	jpg (Q = 65)	None	0.299	0.044	29.7	0.105
		0	png (lossless)	None	0.338	0.060	28.3	0.090
		1000	png (lossless)	CA*	0.424	0.080	24.6	0.119
EDSR	NTIRE 2022	unknown	jpg (Q unknown)	None	0.340	0.051	27.5	0.095
	Synthesized	0	jpg (Q = 65)	None	0.473	0.064	25.8	0.104
		0	png (lossless)	None	0.474	0.074	24.5	0.096
		1000	png (lossless)	CA*	0.421	0.066	25.5	0.132
HRNet	NTIRE 2022	unknown	jpg (Q unknown)	None	0.376	0.065	25.4	0.102
	Synthesized	0	jpg (Q = 65)	None	0.397	0.066	25.3	0.108
		0	png (lossless)	None	0.411	0.070	25.0	0.101
		1000	png (lossless)	CA*	0.514	0.078	23.9	0.128
HSCNN+	NTIRE 2022	unknown	jpg (Q unknown)	None	0.391	0.067	25.5	0.105
	Synthesized	0	jpg (Q = 65)	None	0.490	0.073	24.5	0.113
		0	png (lossless)	None	0.485	0.080	23.9	0.101
		1000	png (lossless)	CA*	0.508	0.075	24.4	0.148

*CA: chromatic aberration, from a patent double Gauss lens (US20210263286A1).

TABLE S.II: Evaluation of pre-trained models on synthesized validation data generated from the ARAD1K dataset (Part II).

Network	Data property				MRAE ↓	RMSE ↓	PSNR ↑	SAM ↓
	Data source	Noise (npe)	RGB format	Aberration				
HySAT	NTIRE 2022	unknown	jpg (Q unknown)	None	0.176	0.028	34.6	0.085
	Synthesized	0	jpg (Q = 65)	None	0.438	0.047	29.5	0.087
		0	png (lossless)	None	0.355	0.055	29.1	0.083
		1000	png (lossless)	CA*	0.326	0.047	29.4	0.127
HPRN	NTIRE 2022	unknown	jpg (Q unknown)	None	0.257	0.044	30.4	0.098
	Synthesized	0	jpg (Q = 65)	None	0.456	0.056	28.1	0.106
		0	png (lossless)	None	0.383	0.067	27.1	0.102
		1000	png (lossless)	CA*	0.524	0.104	22.0	0.130
SSTHyper	NTIRE 2022	unknown	jpg (Q unknown)	None	0.181	0.030	33.6	0.083
	Synthesized	0	jpg (Q = 65)	None	0.439	0.047	29.7	0.088
		0	png (lossless)	None	0.367	0.055	29.0	0.082
		1000	png (lossless)	CA*	0.314	0.058	27.7	0.117
MSFN	NTIRE 2022	unknown	jpg (Q unknown)	None	0.226	0.038	31.9	0.084
	Synthesized	0	jpg (Q = 65)	None	0.366	0.043	30.2	0.090
		0	png (lossless)	None	0.360	0.056	28.6	0.085
		1000	png (lossless)	CA*	0.328	0.055	28.3	0.119
GMSR	NTIRE 2022	unknown	jpg (Q unknown)	None	0.308	0.056	27.5	0.113
	Synthesized	0	jpg (Q = 65)	None	0.366	0.043	30.2	0.090
		0	png (lossless)	None	0.342	0.062	26.9	0.110
		1000	png (lossless)	CA*	0.484	0.075	24.9	0.138
SSRNet	NTIRE 2022	unknown	jpg (Q unknown)	None	0.270	0.048	29.5	0.097
	Synthesized	0	jpg (Q = 65)	None	0.301	0.051	29.1	0.103
		0	png (lossless)	None	0.356	0.058	27.8	0.096
		1000	png (lossless)	CA*	0.419	0.075	25.8	0.130

*CA: chromatic aberration, from a patent double Gauss lens (US20210263286A1).

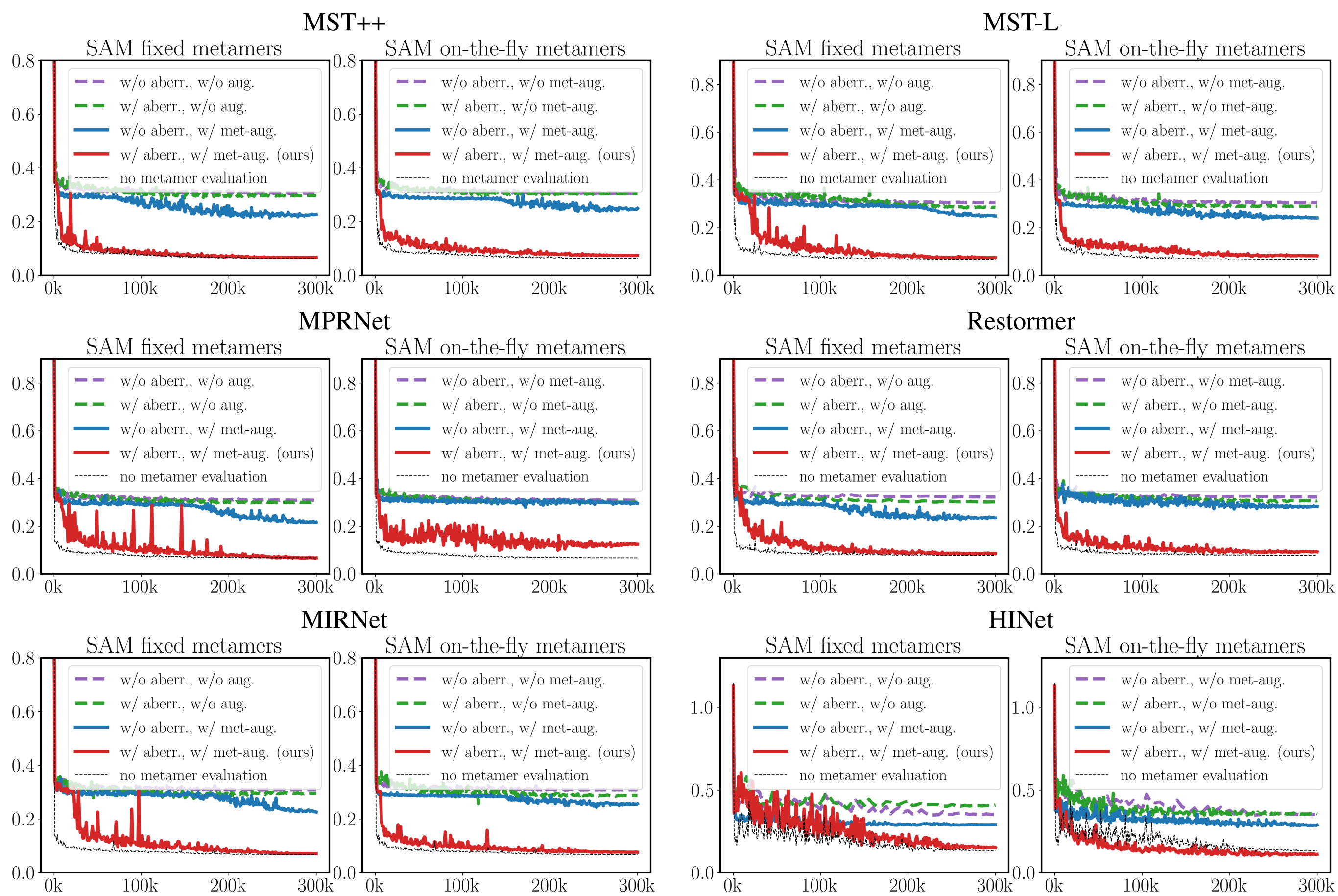

Fig. S5: Chromatic aberrations improve spectral accuracy for MST++, MST-L, MPRNet, Restormer, MIRNet, and HINet. In each group, left: fixed metamers, and right: on-the-fly metamers.

TABLE S.III: Cross-dataset validation for all networks (Part I).

		MST++ [4]				MST-L [3]			
Trained on	Validated on	MRAE↓	RMSE↓	PSNR↑	SAM↓	MRAE↓	RMSE↓	PSNR↑	SAM↓
CAVE	CAVE	0.237	0.034	31.9	0.194	0.234	0.031	32.0	0.187
ARAD1K	CAVE	1.626	0.074	24.4	0.376	2.055	0.070	25.3	0.367
ICVL	ICVL	0.079	0.019	38.3	0.024	0.063	0.015	41.1	0.023
ARAD1K	ICVL	1.032	0.188	19.3	0.924	0.349	0.052	27.8	0.100
KAUST	KAUST	0.069	0.013	44.4	0.061	0.082	0.016	43.8	0.070
ARAD1K	KAUST	1.042	0.100	22.0	0.370	1.114	0.115	21.8	0.370
		MPRNet [17]				Restormer [15]			
Trained on	Validated on	MRAE↓	RMSE↓	PSNR↑	SAM↓	MRAE↓	RMSE↓	PSNR↑	SAM↓
CAVE	CAVE	0.295	0.045	29.4	0.173	0.246	0.036	30.0	0.177
ARAD1K	CAVE	2.063	0.060	26.4	0.378	1.689	0.060	26.5	0.375
ICVL	ICVL	0.077	0.018	39.9	0.024	0.084	0.020	37.4	0.026
ARAD1K	ICVL	0.349	0.050	27.5	0.100	0.347	0.052	27.4	0.097
KAUST	KAUST	0.170	0.022	35.8	0.071	0.067	0.014	44.9	0.066
ARAD1K	KAUST	0.885	0.101	23.1	0.350	1.496	0.144	20.0	0.363
		MIRNet [16]				HINet [5]			
Trained on	Validated on	MRAE↓	RMSE↓	PSNR↑	SAM↓	MRAE↓	RMSE↓	PSNR↑	SAM↓
CAVE	CAVE	0.214	0.027	33.6	0.177	0.283	0.041	29.4	0.191
ARAD1K	CAVE	2.039	0.075	24.9	0.406	1.512	0.084	23.3	0.393
ICVL	ICVL	0.060	0.013	40.8	0.023	0.087	0.021	36.2	0.028
ARAD1K	ICVL	0.365	0.052	27.5	0.114	0.387	0.058	26.2	0.127
KAUST	KAUST	0.079	0.015	42.9	0.070	0.089	0.017	42.2	0.074
ARAD1K	KAUST	1.642	0.154	19.4	0.357	1.393	0.140	19.8	0.362
		HDNet [7]				AWAN [9]			
Trained on	Validated on	MRAE↓	RMSE↓	PSNR↑	SAM↓	MRAE↓	RMSE↓	PSNR↑	SAM↓
CAVE	CAVE	0.266	0.041	29.1	0.199	0.305	0.057	28.0	0.237
ARAD1K	CAVE	1.564	0.078	23.9	0.406	1.743	0.077	24.7	0.397
ICVL	ICVL	0.076	0.018	37.4	0.028	0.083	0.018	38.6	0.026
ARAD1K	ICVL	0.598	0.085	22.3	0.129	0.408	0.060	26.5	0.108
KAUST	KAUST	0.076	0.015	42.0	0.070	0.083	0.015	41.0	0.063
ARAD1K	KAUST	1.389	0.142	19.6	0.394	1.844	0.174	18.7	0.370
		EDSR [11]				HRNet [18]			
Trained on	Validated on	MRAE↓	RMSE↓	PSNR↑	SAM↓	MRAE↓	RMSE↓	PSNR↑	SAM↓
CAVE	CAVE	0.308	0.058	26.1	0.194	0.317	0.058	26.7	0.196
ARAD1K	CAVE	1.757	0.078	23.4	0.416	1.170	0.076	23.8	0.389
ICVL	ICVL	0.111	0.030	33.0	0.027	0.103	0.026	33.8	0.028
ARAD1K	ICVL	0.474	0.067	24.2	0.119	0.531	0.075	23.3	0.115
KAUST	KAUST	0.215	0.037	31.6	0.081	0.094	0.020	39.2	0.069
ARAD1K	KAUST	1.391	0.145	19.4	0.408	1.202	0.127	20.6	0.412
		HSCNN+ [12]							
Trained on	Validated on	MRAE↓	RMSE↓	PSNR↑	SAM↓				
CAVE	CAVE	0.328	0.067	25.4	0.222				
ARAD1K	CAVE	2.522	0.098	21.1	0.419				
ICVL	ICVL	0.223	0.042	28.9	0.029				
ARAD1K	ICVL	0.528	0.074	23.3	0.117				
KAUST	KAUST	2.093	0.192	19.5	0.075				
ARAD1K	KAUST	1.281	0.135	19.9	0.351				

TABLE S.IV: Cross-dataset validation for all networks (Part II).

		HySAT				HPRN			
Trained on	Validated on	MRAE↓	RMSE↓	PSNR↑	SAM↓	MRAE↓	RMSE↓	PSNR↑	SAM↓
CAVE	CAVE	0.286	0.043	28.7	0.202	0.265	0.039	30.4	0.181
ARAD1K	CAVE	1.250	0.088	23.7	0.376	1.057	0.111	21.0	0.424
ICVL	ICVL	0.071	0.017	39.1	0.026	0.089	0.019	39.6	0.026
ARAD1K	ICVL	0.428	0.054	26.6	0.114	0.418	0.056	26.6	0.130
KAUST	KAUST	0.066	0.013	44.9	0.058	0.078	0.015	42.5	0.067
ARAD1K	KAUST	1.057	0.107	21.8	0.366	1.357	0.144	19.8	0.370
		SSTHyper				MSFN			
Trained on	Validated on	MRAE↓	RMSE↓	PSNR↑	SAM↓	MRAE↓	RMSE↓	PSNR↑	SAM↓
CAVE	CAVE	0.232	0.035	31.2	0.176	0.24	0.035	31.3	0.191
ARAD1K	CAVE	1.036	0.091	22.9	0.399	0.948	0.093	22.9	0.387
ICVL	ICVL	0.056	0.011	41.7	0.022	0.074	0.017	39.5	0.023
ARAD1K	ICVL	0.430	0.054	26.5	0.112	0.397	0.053	27.8	0.124
KAUST	KAUST	0.079	0.015	43.7	0.064	0.076	0.014	44.7	0.064
ARAD1K	KAUST	1.052	0.106	22.2	0.400	1.213	0.122	20.9	0.383
		GMSR				SSRNet			
Trained on	Validated on	MRAE↓	RMSE↓	PSNR↑	SAM↓	MRAE↓	RMSE↓	PSNR↑	SAM↓
CAVE	CAVE	0.309	0.052	26.9	0.199	0.250	0.032	31.9	0.195
ARAD1K	CAVE	0.971	0.120	19.5	0.441	1.097	0.072	25.8	0.394
ICVL	ICVL	0.083	0.022	36.0	0.033	0.102	0.024	37.1	0.030
ARAD1K	ICVL	0.574	0.079	23.1	0.125	0.478	0.064	25.3	0.149
KAUST	KAUST	0.090	0.018	39.3	0.083	0.083	0.016	42.0	0.082
ARAD1K	KAUST	0.883	0.087	23.0	0.357	1.039	0.106	21.6	0.378

TABLE S.V: Training with metamers on the CAVE, ICVL, and KAUST datasets. Part I: MST++, MST-L, MPRNet, Restormer, MIRNet, and HINet.

		MST++ [4]				MST-L [3]			
Dataset	Metamer	MRAE↓	RMSE↓	PSNR↑	SAM↓	MRAE↓	RMSE↓	PSNR↑	SAM↓
CAVE [14]	no	1.014	0.038	29.9	0.192	0.932	0.057	26.1	0.195
	fixed	38.26	0.053	29.6	0.229	66.470	0.062	27.6	0.295
	on-the-fly	226.0	0.078	25.2	0.451	286.557	0.085	24.7	0.504
ICVL [1]	no	0.067	0.016	40.1	0.027	0.067	0.015	39.8	0.025
	fixed	1.454	0.041	34.8	0.229	2.080	0.040	34.5	0.28
	on-the-fly	2.615	0.087	24.3	0.268	3.281	0.087	23.7	0.261
KAUST [10]	no	0.082	0.016	43.2	0.076	0.097	0.017	42.0	0.074
	fixed	2.033	0.022	39.0	0.217	1.920	0.022	38.8	0.219
	on-the-fly	1.874	0.032	33.7	0.245	4.235	0.023	39.8	0.236
		MPRNet [17]				Restormer [15]			
Dataset	Metamer	MRAE↓	RMSE↓	PSNR↑	SAM↓	MRAE↓	RMSE↓	PSNR↑	SAM↓
CAVE [14]	no	1.110	0.041	30.3	0.177	0.987	0.040	29.5	0.175
	fixed	34.272	0.046	32.3	0.209	93.697	0.047	34.7	0.276
	on-the-fly	355.958	0.112	22.8	0.626	379.277	0.093	25.7	0.501
ICVL [1]	no	0.084	0.019	38.2	0.025	0.083	0.020	38.2	0.026
	fixed	1.693	0.041	33.4	0.228	1.730	0.040	34.7	0.228
	on-the-fly	2.584	0.094	22.9	0.259	2.254	0.099	22.7	0.272
KAUST [10]	no	0.071	0.013	43.6	0.066	0.063	0.013	44.6	0.063
	fixed	2.668	0.024	35.7	0.216	2.077	0.020	40.3	0.213
	on-the-fly	2.431	0.037	32.2	0.251	2.623	0.032	34.1	0.281
		MIRNet [16]				HINet [5]			
Dataset	Metamer	MRAE↓	RMSE↓	PSNR↑	SAM↓	MRAE↓	RMSE↓	PSNR↑	SAM↓
CAVE [14]	no	1.167	0.035	31.5	0.190	1.064	0.050	27.3	0.196
	fixed	29.483	0.044	31.7	0.212	55.259	0.056	29.2	0.223
	on-the-fly	131.464	0.083	25.0	0.405	141.691	0.072	27.5	0.362
ICVL [1]	no	0.070	0.015	39.7	0.025	0.071	0.017	38.9	0.027
	fixed	3.794	0.038	35.0	0.227	2.445	0.041	34.8	0.228
	on-the-fly	2.895	0.095	23.0	0.265	3.600	0.092	23.4	0.271
KAUST [10]	no	0.078	0.015	42.2	0.069	0.097	0.017	41.9	0.080
	fixed	2.072	0.021	38.7	0.216	2.481	0.023	37.5	0.218
	on-the-fly	2.312	0.037	33.1	0.257	4.323	0.023	38.9	0.229

TABLE S.VI: Training with metamers on the CAVE, ICVL, and KAUST datasets. Part II: HDNet, AWAN, MIRNet, HINet, and HSCNN+.

		HDNet [7]				AWAN [9]			
Dataset	Metamer	MRAE↓	RMSE↓	PSNR↑	SAM↓	MRAE↓	RMSE↓	PSNR↑	SAM↓
CAVE [14]	no	1.071	0.043	29.4	0.197	1.045	0.069	24.7	0.208
	fixed	56.996	0.071	26.8	0.298	88.236	0.072	28.8	0.291
	on-the-fly	78.524	0.093	23.8	0.274	259.101	0.079	26.7	0.366
ICVL [1]	no	0.076	0.019	37.2	0.027	0.100	0.020	37.9	0.028
	fixed	2.786	0.039	34.0	0.226	3.034	0.040	34.3	0.230
	on-the-fly	2.891	0.091	23.3	0.259	2.707	0.094	22.8	0.280
KAUST [10]	no	0.085	0.017	40.8	0.082	0.101	0.017	39.6	0.105
	fixed	2.891	0.022	37.9	0.217	2.152	0.021	38.3	0.221
	on-the-fly	3.789	0.023	38.9	0.233	3.855	0.024	38.2	0.233
		EDSR [11]				HRNet [18]			
Dataset	Metamer	MRAE↓	RMSE↓	PSNR↑	SAM↓	MRAE↓	RMSE↓	PSNR↑	SAM↓
CAVE [14]	no	1.207	0.057	26.3	0.202	1.087	0.056	26.6	0.198
	fixed	54.125	0.066	27.0	0.292	106.082	0.065	27.3	0.310
	on-the-fly	199.916	0.106	21.2	0.371	151.295	0.100	21.8	0.356
ICVL [1]	no	0.112	0.029	32.9	0.028	0.106	0.027	33.3	0.029
	fixed	2.275	0.045	30.5	0.227	2.182	0.045	30.8	0.228
	on-the-fly	2.721	0.093	23.0	0.262	2.703	0.083	24.0	0.244
KAUST [10]	no	0.260	0.044	30.5	0.085	0.097	0.021	37.8	0.070
	fixed	2.002	0.033	32.2	0.218	2.819	0.024	37.5	0.218
	on-the-fly	3.883	0.025	36.1	0.221	3.373	0.026	36.9	0.223
		HSCNN+ [12]							
Dataset	Metamer	MRAE↓	RMSE↓	PSNR↑	SAM↓				
CAVE [14]	no	1.027	0.065	25.3	0.229				
	fixed	55.611	0.076	25.1	0.313				
	on-the-fly	154.416	0.104	21.8	0.353				
ICVL [1]	no	0.226	0.043	28.6	0.030				
	fixed	1.908	0.052	28.1	0.229				
	on-the-fly	1.627	0.102	21.9	0.253				
KAUST [10]	no	1.832	0.171	19.9	0.077				
	fixed	6.240	0.166	20.6	0.217				
	on-the-fly	2.669	0.057	25.9	0.222				

TABLE S.VII: Training with metamers on the CAVE, ICVL, and KAUST datasets. Part III: HySAT, HPRN, SSTHyper, MSFN, GMSR, and SSRNet.

		HySAT				HPRN			
Dataset	Metamer	MRAE↓	RMSE↓	PSNR↑	SAM↓	MRAE↓	RMSE↓	PSNR↑	SAM↓
CAVE [14]	no	1.088	0.035	31.8	0.184	0.900	0.043	29.3	0.196
	fixed	218.925	0.065	28.1	0.372	76.216	0.062	27.7	0.314
	on-the-fly	338.654	0.087	25.0	0.487	352.391	0.106	23.2	0.512
ICVL [1]	no	0.080	0.020	38.9	0.026	0.081	0.018	38.4	0.026
	fixed	3.100	0.042	32.9	0.228	2.543	0.042	34.1	0.232
	on-the-fly	3.044	0.092	23.1	0.260	2.367	0.098	22.7	0.265
KAUST [10]	no	0.070	0.013	43.7	0.073	0.109	0.020	40.9	0.078
	fixed	2.895	0.021	39.1	0.216	2.989	0.025	37.5	0.221
	on-the-fly	4.553	0.026	36.9	0.241	3.836	0.025	38.3	0.246
		SSTHyper				MSFN			
Dataset	Metamer	MRAE↓	RMSE↓	PSNR↑	SAM↓	MRAE↓	RMSE↓	PSNR↑	SAM↓
CAVE [14]	no	1.190	0.032	32.8	0.182	0.863	0.037	30.8	0.189
	fixed	98.149	0.066	28.2	0.313	96.891	0.060	31.2	0.303
	on-the-fly	398.022	0.097	24.2	0.558	44.497	0.067	26.9	0.224
ICVL [1]	no	0.058	0.014	41.3	0.025	0.078	0.019	38.1	0.025
	fixed	3.080	0.039	35.1	0.225	2.141	0.041	34.3	0.226
	on-the-fly	2.160	0.094	23.1	0.256	2.801	0.084	24.3	0.250
KAUST [10]	no	0.075	0.014	43.6	0.063	0.075	0.014	43.8	0.069
	fixed	1.965	0.021	39.5	0.216	2.395	0.021	39.1	0.216
	on-the-fly	4.441	0.036	33.8	0.235	3.971	0.021	39.9	0.227
		GMSR				SSRNet			
Dataset	Metamer	MRAE↓	RMSE↓	PSNR↑	SAM↓	MRAE↓	RMSE↓	PSNR↑	SAM↓
CAVE [14]	no	1.302	0.035	31.2	0.193	1.114	0.042	29.8	0.203
	fixed	105.385	0.052	30.4	0.328	117.309	0.055	31.0	0.294
	on-the-fly	195.193	0.073	24.9	0.319	56.450	0.053	29.0	0.231
ICVL [1]	no	0.093	0.024	35.0	0.034	0.098	0.022	37.6	0.030
	fixed	1.845	0.043	32.3	0.230	2.023	0.040	34.2	0.229
	on-the-fly	2.770	0.071	25.9	0.238	2.526	0.075	25.0	0.237
KAUST [10]	no	0.152	0.025	36.8	0.094	0.114	0.019	41.7	0.085
	fixed	2.411	0.024	35.9	0.223	2.155	0.022	38.7	0.216
	on-the-fly	3.810	0.023	38.5	0.221	4.099	0.022	39.6	0.221

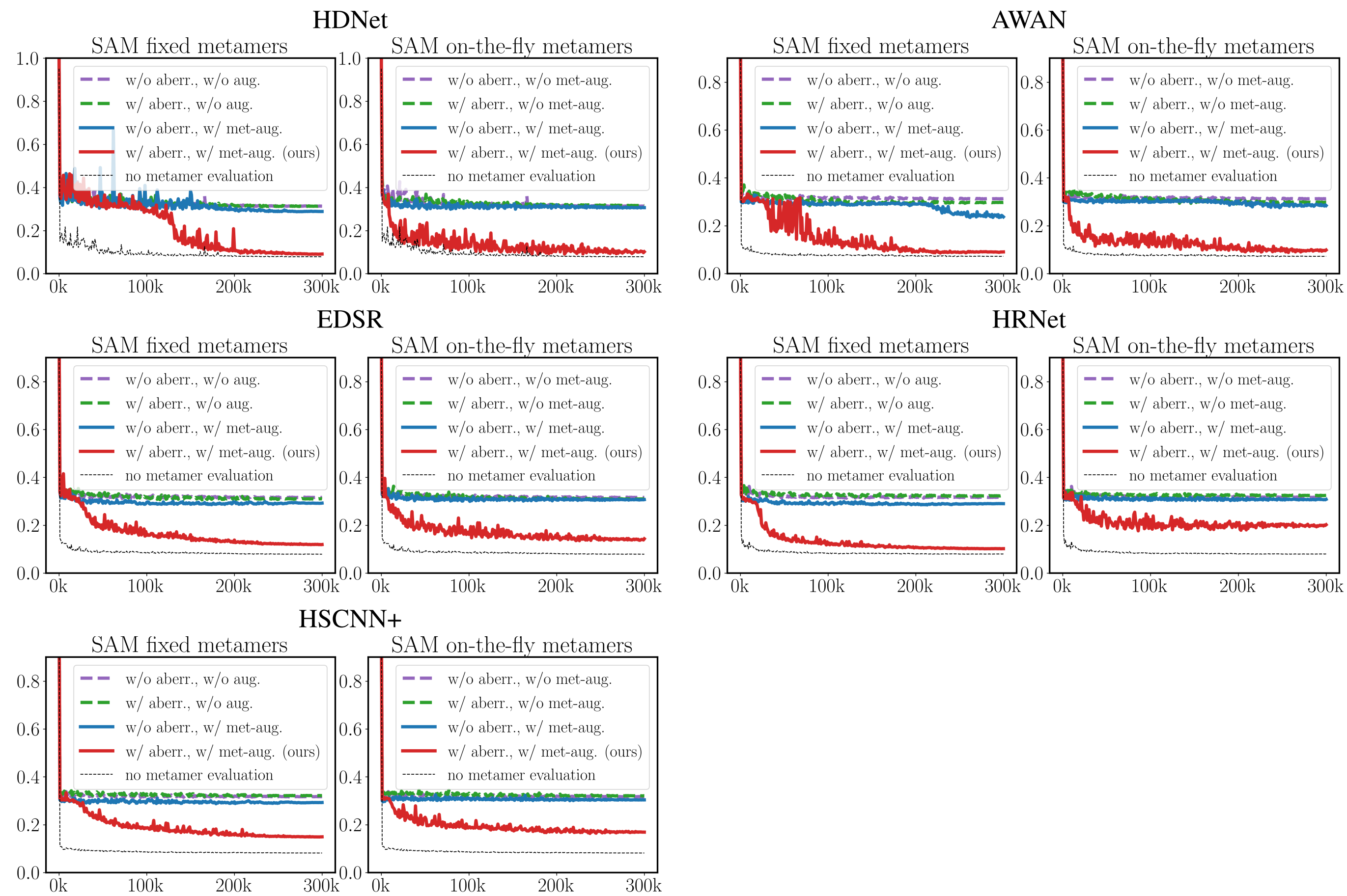

Fig. S6: The aberration advantage results for HDNet, AWAN, EDSR, HRNet, and HSCNN+ on ARAD1K. In each group, left is for fixed metamers, and right is for on-the-fly metamers.

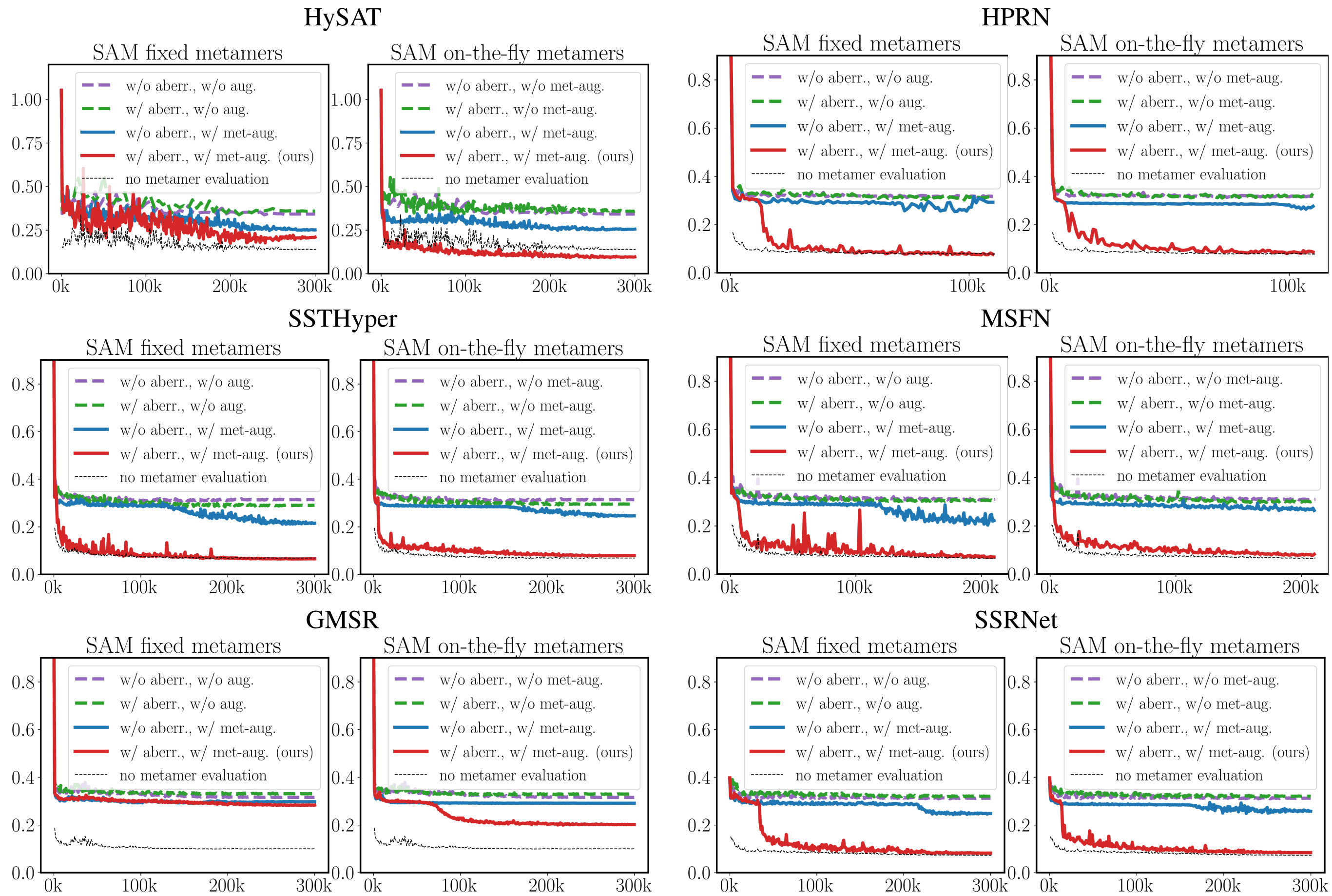

Fig. S7: Chromatic aberrations improve spectral accuracy for HySAT, HPRN*, SSTHyper, MSFN**, GMSR, and SSRNet. In each group, left: fixed metamers, and right: on-the-fly metamers. * For HPRN, we followed the training strategy and observed divergence after 100k iterations. Converged results are reported here at 100k iterations. ** For MSFN, it takes >72h to reach 200k, but we have observed convergence, so the results are reported at 200k iterations.

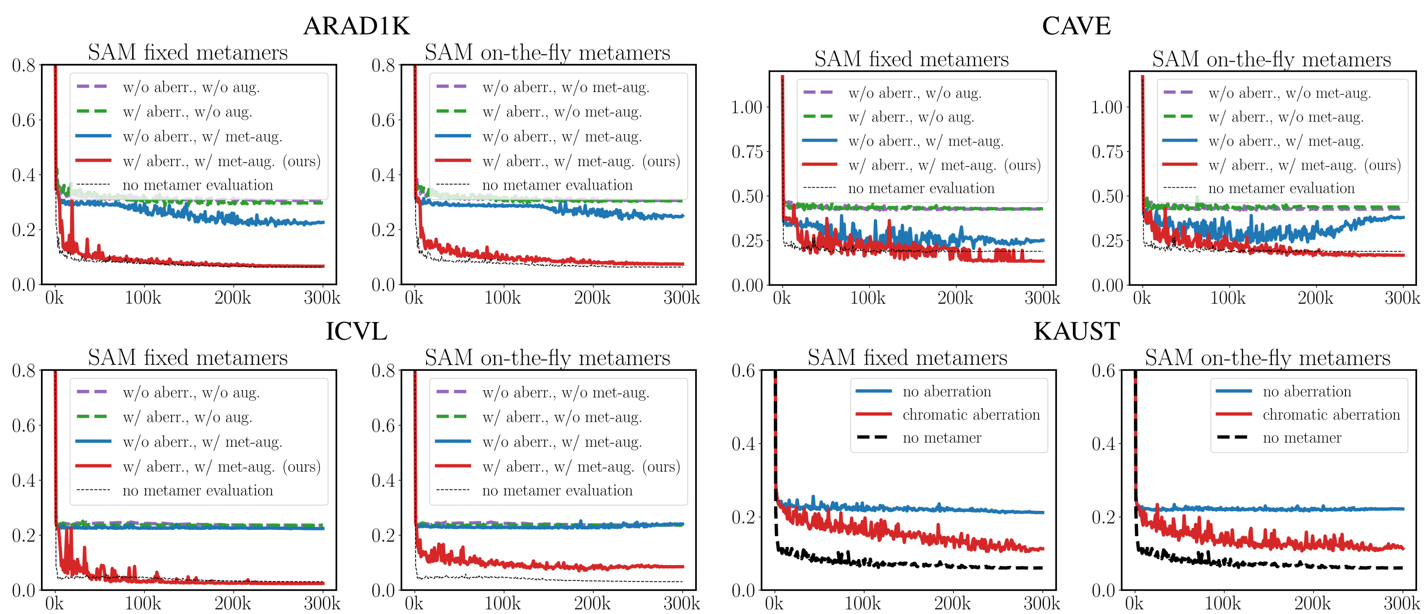

Fig. S8: The aberration advantage results for MST++ on all datasets. In each group, left is for fixed metamers, and right is for on-the-fly metamers.